Thrust Loss Due to Plume Impingement Effects

E. Mayer,* J. Hermel,† and A. W. Rogers‡
Hughes Aircraft Company, El Segundo, California

The impingement of a thruster exhaust plume on spacecraft structures generally results in a thrust loss depending on the configuration of the surfaces affected. Calculations of the thrust loss resulting from internal impingement of a plume, including the effect of the nozzle boundary layer, with a nearly coaxial cylinder are performed by three analytical methods: method of characteristics, Monte Carlo, and a source-flow method convenient for rapid assessment of thrust loss. For impingement in the transitional-flow regime, a "bridging relation" applicable to shear flow is used to modify the impingement effect calculated for the free-molecule regime. Results are given for the Hughes 5-lbf thruster plume within the HS 376 cylindrical solar panel. Reasonable agreement of the calculated thrust loss is obtained with flight data from HS 376-class spacecraft. A prediction is also made for the plume of the highly viscous nozzle flow from a small electrothermal thruster.

Nomenclature

A^* = nozzle throat area
B = plume density parameter
B' = source-flow plume-density parameter
c^* = characteristic velocity
C_F = thrust coefficient
d^* = nozzle throat diameter
F = thrust
ΔF = total thrust loss
ΔF_δ = cant angle component of thrust loss
ΔF_τ = plume shear component of thrust loss
g = gravity acceleration
H = nozzle axis uncanted offset
I_{sp} = specific impulse
Kn = Knudsen number
ℓ = reference length
L = impingement length
M = bridging function
$\mathfrak{M}$ = molecular weight
p = pressure
r = radial distance measured from nozzle exit center
r_e = nozzle exit radius
R = cylinder internal radius
S = surface impingement area
Δt = small time increment
$\bar{T}$ = average stagnation temperature
T_s = impingement surface temperature
V = plume velocity
ΔV = spacecraft-maneuver speed change
V_m = maximum velocity in fully expanded plume
$\dot{W}$ = total mass flow rate
$\dot{W}_b$ = boundary-layer mass flow rate
x = axial distance measured from nozzle exit
α, β = source-flow parameters
γ = specific heat ratio
δ = nozzle axis cant angle
ϵ = nozzle area ratio
θ = flow angle referred to plume axis
θ_e = nozzle exit angle
λ = mean free path
ρ = plume density
ρ_a = plume density along axis
τ = transitional flow shear stress
τ_{FM} = free-molecule flow shear stress
ϕ = incidence angle of plume velocity vector at impingement surface

Subscripts

b = boundary layer
c = inviscid core flow
e = nozzle exit plane
i = ideal limit
0 = stagnation or chamber value

I. Introduction

A PERENNIAL task in the design of spacecraft propulsion systems is to minimize the adverse effects of rocket plume impingement on neighboring spacecraft structures. Of particular interest in the Hughes HS 376-class spacecraft is the impingement of the plume on the interior of a cylindrical solar panel within which a pair of 5-lbf hydrazine-decomposition thrusters operate in orbital flight. As shown in Figs. 1 and 2, solar power generation is enhanced in the design of this dual-spin-stabilized spacecraft by telescoping two concentric cyl-

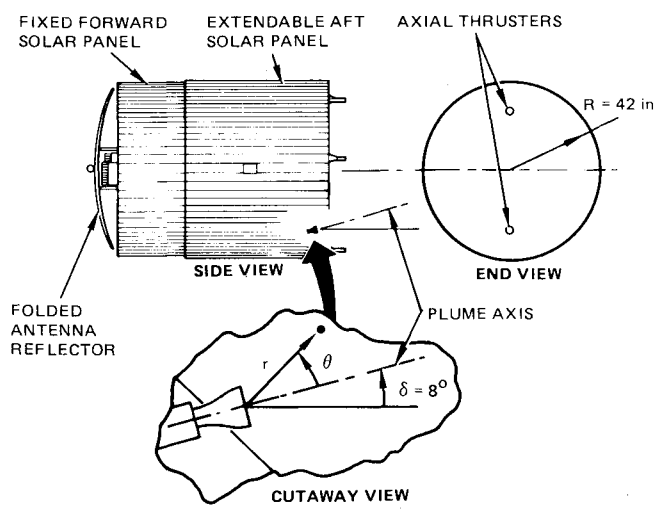

Fig. 1 Stowed HS 376 spacecraft with two canted axial thrusters near base of fixed forward solar panel and definition of polar coordinate system (r,θ).

Presented as Paper 85-1157 at the AIAA/SAE/ASME/ASEE 21st Joint Propulsion Conference, Monterey, CA, July 8-10, 1985; received July 29, 1985; revision received Feb. 18, 1986.

*Senior Scientist, Engineering Mechanics Laboratory, Space and Communications Group. Member AIAA.

†Senior Staff Engineer, Propulsion Systems Laboratory, Space and Communications Group. Member AIAA.

‡ Senior Scientist, Engineering Mechanics Laboratory, Space and Communications Group. Member AIAA.

inders covered with solar cells. Figure 1 shows the stowed launch configuration and the inner cylinder with the two axially directed thrusters exposed. During orbital operation, the outer cylinder is extended, as shown in Fig. 2, and is subject to plume impingement from the thrusters that remain fixed near the cylinder base. The plume shear against the interior cylindrical surface results in an effective thrust loss, while plume impingement against the cylinder base generally has a negligible effect on the net axial thrust. The sum of the plume shear loss, as modified by any base pressure contribution, and the loss due to thruster cant angle δ determines the total "installed" thrust loss. Plume interaction effects are considered negligible.

The plume analysis methods and plume shear evaluation technique requiring treatment of transitional flow are described in Sec. II. In the calculation of the plume and its impingement effects, the choice of analytical approach is usually dictated by accuracy, computational time, and cost factors. Considering these factors, the method of characteristics, described in Sec. II, was used as a baseline procedure in the HS 376 plume calculations because it is a reasonably inexpensive yet relatively accurate method. To obtain independent assessment of plume impingement effects, the more fundamental, but computationally time-consuming and expensive Monte Carlo method was used. Finally, a source-flow method, useful in approximating the mass flux in the plume far field, is presented in Sec. II. This method is described in detail, because it offers in a simple and flexible analytical framework the advantages of formulas for predicting plume flowfield properties with propulsion engineering test data, such as c^* efficiency and thrust coefficient C_F when the latter are available.

Plume flowfield and thrust loss predictions for these three methods are compared in Sec. III.

Section IV concludes that, for thrust loss predictions applied to the extended interior surfaces of the HS 376 solar panel, the results of various approaches agree substantially with observed flight data. For far-field impingement effects, the source-flow method described herein seems particularly useful in preliminary design calculations because of its flexibility and relative accuracy.

II. Methodology

Method of Characteristics

The standard procedure for calculating rocket exhaust plume expansion into an ambient atmosphere is the supersonic method of characteristics. The specific analyses of gaseous plume expansion presented here make use of an axisymmetric, isentropic, constant specific heat ratio computer code. Although the plume is considered inviscid, the effect of nozzle boundary layer on subsequent expansion into a vacuum is included. For larger motors with turbulent boundary layers at the nozzle exit plane (e.g., apogee kick motors), a correlation method based on Ref. 1 supplies the required boundary-layer properties. Laminar exit plane boundary-layer properties for smaller thrusters, such as the Hughes 5-lbf hydrazine-decomposition thruster, are calculated using Whitfield's code.[2] Actual exit plane boundary-layer properties near the nozzle lip are partially replaced by a computed equivalent Mach number 1.05 sublayer that conserves mass and momentum of the original layer. This replacement is required to input purely supersonic flow variables into the method-of-characteristics code.

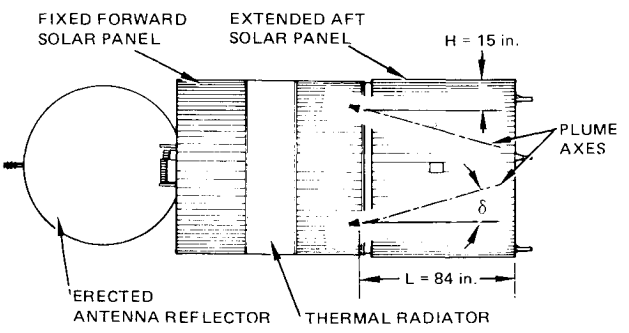

Fig. 2 HS 376 spacecraft in full-up configuration.

Input to the method-of-characteristics code specifies "exit plane" conditions on a spherical cap. The input consists of stagnation pressure and temperature, exit plane specific heat ratio and gas molecular weight, exit pressure and velocity distribution, nozzle lip angle and exit radius, and several computation parameters controlling mesh size, radial and axial extent of the flowfield, and allowable increments in calculated variables. Automatic mesh reduction, by insertion of additional characteristic lines, is provided. Output data are the left-running characteristic lines, and the pressure, density, temperature, velocity, Mach number, flow direction, cumulative mass flow, and stagnation pressure along those lines. Thrust corresponding to the exit plane input data is computed so that calculated impingement forces can be expressed in ratio to thrust.

Source-Flow Method

In parallel with the method-of-characteristics description of the plume, an alternative approximate analysis of the axially symmetric far field was developed for rapid assessment of plume impingement effects on extended surface areas relatively far from the nozzle exit. In polar coordinates (r, θ) with the origin at the nozzle exit center, as shown in Fig. 1, the dependence of the axisymmetric plume density is described by a three-parameter (α, β, V_m) form of the source flow:

$$\rho(r,\theta) = \left[\alpha\left(\cos\frac{\theta}{2}\right)^{\beta}\right] \Big/ V_m r^2 \tag{1}$$

where V_m is the maximum velocity, directed along r, attained in the far field. It follows, as developed in greater detail in the Appendix, that α and β can be related to the total mass flow rate $\dot{W}$ and thrust F by conservation laws

$$\dot{W} = \frac{8\pi\alpha}{\beta+2} \tag{2}$$

$$F = \frac{\beta}{\beta+4}\dot{W}\frac{V_m}{g} \tag{3}$$

while V_m is, in principle, related to the maximum "ideal" specific impulse $I_{sp,i}$ obtainable from the propellants upon combustion and expansion to vacuum

$$V_m = gI_{sp,i} \tag{4}$$

To evaluate the parameters α and β and the velocity V_m introduced in Eq. (1), propulsion test data and/or analytical predictions of nozzle flow properties can be employed in Eqs. (2–4). In the source-flow approximation, it is desirable to make maximum use of propulsion test data for calculating these parameters. In particular, the effect of incomplete combustion implicit in test data on p_0 and $\dot{W}$ which yield the value of the characteristic velocity

$$c^* = gp_0A^*/\dot{W}$$

is included in the definition of the "ideal" $I_{sp,i}$ in Eq. (4)

$$I_{sp,i} = C_{F,i}c^*/g$$

By using the propulsion parameters $I_{sp} = F/\dot{W}$ and $C_F = F/p_0A^*$, Eq. (3) can be formulated to show the effect of

nozzle efficiency on β

$$\frac{\beta}{\beta+4}=\frac{C_F}{C_{F,i}}=\frac{I_{sp}}{I_{sp,i}} \tag{5}$$

Thus with increasing nozzle efficiency $C_F/C_{F,i}\to 1$, the parameter $\beta\to\infty$, and, therefore, the plume mass flux ρV_m in Eq. (1) [being proportional to the factor $[\cos(\theta/2)^\beta]$ is confined to the axial direction. Conversely, divergence of the plume mass flux depends on the ratio $C_F/C_{F,i}<1$. The mass flux divergence in the far field is described by the reduced density (independent of r and V_m) from Eq. (1)

$$\frac{\rho(r,\theta)}{\rho(r,0)}=\frac{\rho}{\rho_a}=\left(\cos\frac{\theta}{2}\right)^\beta \tag{6}$$

where ρ_a is the density along the plume axis.

In a purely analytical calculation of β, the ratio $C_F/C_{F,i}$ is readily calculated for one-dimensional, inviscid, conical nozzle flow. The ideal thrust coefficient depends only on the specific heat ratio γ (e.g., Ref. 3), expressed as

$$C_{F,i}=\sqrt{\frac{2\gamma^2}{\gamma-1}\left(\frac{2}{\gamma+1}\right)^{(\gamma+1)/(\gamma-1)}} \tag{7}$$

and the effect of area ratio ϵ and exit (semivertex) angle θ_e yield the ratio

$$\frac{C_F}{C_{F,i}}=\left(\frac{1+\cos\theta_e}{2}\right)\sqrt{1-\left(\frac{p_e}{p_0}\right)^{(\gamma-1)/\gamma}}+\frac{p_e}{p_0}\frac{\epsilon}{C_{F,i}} \tag{8}$$

where the pressure ratio p_e/p_0 is determined from compressible flow relations as a function of ϵ and γ. Using Eqs. (7) and (8), the values of β have been plotted in Fig. 3 as a function of ϵ, γ, and θ_e.

Inclusion of viscous nozzle flow effects on the far field was made by considering the boundary-layer flow as a perturbation source flow with assumed exit sonic flow, i.e., $\epsilon=1$, superimposed on the inviscid flow. For this application, the magnitude of the perturbing mass flow rate $\dot{W}_b$ can be ascertained either by nozzle flow analysis or estimated from test data on C_F in the approximation

$$\frac{\dot{W}_b}{2\dot{W}}\simeq 1-\frac{C_F}{C_{F,i}}, \qquad \dot{W}_b/\dot{W}\ll 1$$

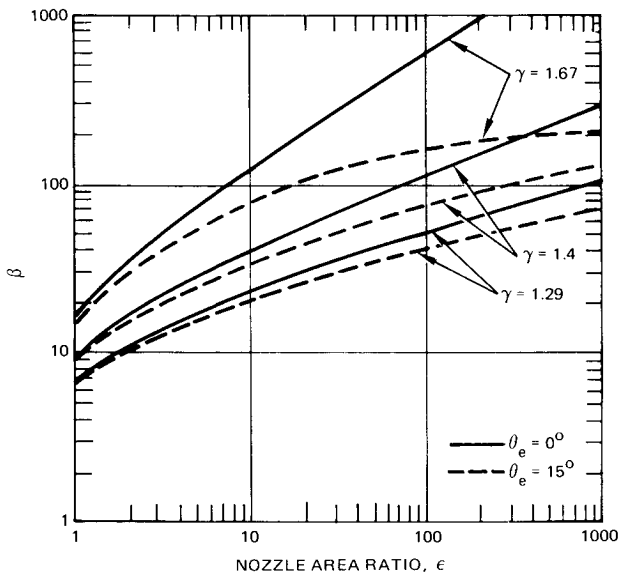

Fig. 3 Source-flow parameter β vs ϵ for several values of specific heat ratio γ and nozzle exit angle θ_e.

The linear superposition leads to two sets of α,β parameters as an extension of Eq. (6) to the far field. A formulation of the superimposed viscous and inviscid flow components of the far-field density is given in the Appendix.

A comparison of the inviscid source-flow density is given in Sec. III with method-of-characteristics density values noted in Ref. 4. Comparisons, including boundary-layer effects, are also illustrated in Sec. III.

Finally, for highly viscous, low-pressure nozzle flows, such as electrothermal thruster flows that contain no inviscid core, given averaged nozzle exit conditions may be adapted for the far-field calculation by the source-flow method. Section III illustrates the source-flow plume prediction for an electrothermal thruster.

Transitional Flow Bridging Relation

In the process of calculating shear stress along a spacecraft surface caused by plume impingement, it was found expedient to use Newtonian impact free-molecule shear equations as a simple first approximation, obtaining an upper limit of estimated thrust loss; however, the calculated mean free path, λ, of impinging gas molecules showed regions where those paths could be quite large when compared, for example, to the diameter of the HS 376 deployed solar cylinder. For this reason, a local Knudsen number, $Kn=\lambda/\ell$, was defined, based on a "local tube radius" analogy, using the transverse distance ℓ between the plume axis and cylinder wall in the plane perpendicular to the plume axis. A local correction (reduction) of free-molecule shear stress, τ_{FM}, is then applied as a function of this Knudsen number to account for transitional τ rather than free-molecule shear stress. For simple, heuristic engineering calculations, the bridging relation of Matting,[5] developed for external, blunt-body flows (Fig. 8 of Ref. 5), $\tau/\tau_{FM}=M(\ell/\lambda)$, is adapted here as plotted in Fig. 4. Although to date this method appears to yield shear losses in reasonable agreement with experimental data and with a Monte Carlo calculation (Sec. III), studies continue on other data and methods for treating transitional impinging flows.

Shear Loss

The calculation of the thrust-loss component, ΔF_τ, due to shear flow of the impinging exhaust plume on a surface S, is defined by

$$\Delta F_\tau=\int_S \tau dS=\int_S \tau_{FM}M(\ell/\lambda)dS \tag{9}$$

where the ratio of the transitional flow shear stress, τ, to the free-molecule impingement shear stress, τ_{FM}, is given by the Matting relation as plotted in Fig. 4, and the value τ_{FM} is obtained from the Newtonian impact equation

$$\tau_{FM}=\rho(V^2/g)\sin\phi\cos\phi$$

where V is the local plume velocity with angle of incidence ϕ at the impingement surface. (In the source-flow model, V is the

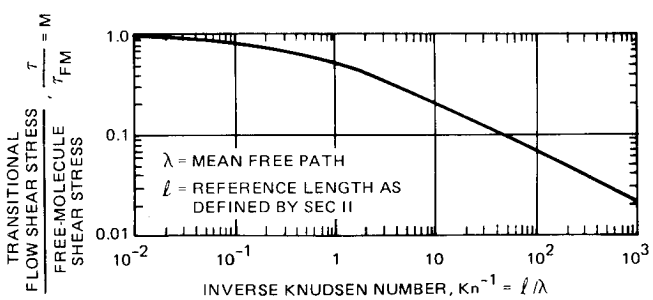

Fig. 4 Bridging between continuum and free-molecule flow (from Ref. 5).

far-field value V_m. See, also, the Appendix.) Evaluation of the integral in Eq. (9) over the interior cylindrical surface S of the HS 376 solar panel requires specification of four parameters: cylinder length L, radius R, radial offset distance H, and nozzle axis cant angle δ.

The total thrust loss, ΔF, is the sum of ΔF_τ and the loss due to cant angle δ, ΔF_δ:

$$\Delta F = \Delta F_\tau + \Delta F_\delta$$

where $\Delta F_\delta = (1 - \cos\delta)F$. Upon calculation of ΔF for several values of δ, the optimum choice of δ is obtained at the minimum value of ΔF.

Monte Carlo Method

While the Matting bridging relation[5] has been applied generally to external shear flows, its application to the present internal flow over a concave solar panel surface is novel. Therefore, a comparison of shear loss predictions with an independent, more fundamental approach such as a Monte Carlo method appeared desirable.

For this purpose, the GAPS (Galileo Axisymmetric Plume Simulation) code[6] was employed in thrust loss calculations for a simple coaxial thruster/spacecraft configuration. The GAPS code makes use of an advanced version of the direct simulation Monte Carlo method orginally developed by Bird.[7] This method is a computational technique for determining the macroscopic characteristics of a real-gas flow from the simulated motion of its molecules. The Monte Carlo calculation starts at time zero along a closed contour within the high-density plume core with flowfield properties determined by the method of characteristics. In subsequent small time increments, Δt, the velocity components and position coordinates of the simulated molecules are modified as the molecules are concurrently followed through representative collisions and boundary interactions in the simulated flowfield. The molecular motion and the collision processes are decoupled by moving the molecules through distances appropriate to their instantaneous velocities in the time interval Δt, and then probabilistically computing a representative set of collisions appropriate to Δt. The calculations are stepped along in time until an equilibrium condition is achieved.

The model assumes hard sphere molecules, diffuse reflection, and complete momentum and energy accommodation of the molecules during collisions with the surface. A distinguishing feature of the GAPS code, in particular, is its imbedded modeling of the highly nonequilibrium flow expanding around the nozzle lip, thus permitting a reasonable simulation of the nozzle backflow.

III. Results

Plume Descriptions

Before comparing the method-of-characteristics, Monte Carlo, and source-flow methods as they apply to real nozzle exhaust flows including viscous effects, inviscid flow calculations of the plume density obtained by the method of characteristics are compared with results based on Eq. (1). An extensive set of such data[4] is expressed by the nondimensional parameter

$$B = \frac{\rho(x)}{\rho_0} \Big/ \left(\frac{d^*}{x}\right)^2 \tag{10}$$

where $\rho(x)$ is the density along the axis, d^* the throat diameter, and ρ_0 refers to stagnation conditions. For given nozzle parameters ϵ, θ_e, and γ, the calculation of $\rho(x)$ by the method of characteristics leads to the values of B given in Ref. 4 and repeated in Table 1. When the analytical one-dimensional form of the source-flow model is applied to the calculation of B, the expression becomes

$$B' = \frac{\sqrt{2}}{64}(\beta+2)\sqrt{(\gamma-1)\left(\frac{2}{\gamma+1}\right)^{(\gamma+1)/(\gamma-1)}} \tag{11}$$

Using the values of $\beta(\epsilon,\theta_e,\gamma)$ obtainable from Eqs. (5), (7), and (8), as given in Fig. 3, the values of β and B' from Eq. (11) are also listed in Table 1. The agreement between the B' values listed in Ref. 4 and the expression in Eq. (11) is satisfactory.

Table 1 Comparison of inviscid flow correlation parameters B and B'

	Data of Ref. 4			Source flow	
θ_e, deg	ϵ	γ	B[a]	β	B'
0	1.0	1.4	0.094[b]	9.3	0.092
	1.0	1.67	0.159[c]	16.1	0.184
	13.8	1.2	0.118	15.7	0.103
	13.8	1.67	1.06[c]	154.7	1.59
15	1.3	1.4	0.103	11.3	0.107
	2.8	1.3	0.117	12.9	0.106
	7.0	1.4	0.25	28.8	0.25
	40.0	1.2	0.155	18.8	0.122
	40.0	1.3	0.29	34.6	0.26
	40.0	1.4	0.59	56.4	0.47
	40.0	1.67	1.04[c]	134.2	1.38
20	15.0	1.2	0.117	13.6	0.091

[a] Unless indicated by footnotes, values of B are given at $x/r_e = 100$.
[b] B evaluated at $x/r_e = 20$; from Ref. 8.
[c] B evaluated at $X/r_e = 50$.

Next, calculation of flowfield properties with boundary-layer effects is illustrated for two nominally 5-lbf hydrazine-decomposition thrusters: one with a conical nozzle having $\epsilon = 100$, $\theta_e = 15$ deg, and nozzle exit radius $r_e = 0.928$ in.; and one with a contoured nozzle having $\epsilon = 300$, $\theta_e = 7.3$ deg, and $r_e = 1.61$ in.

The method-of-characteristics procedure described in Sec. II was applied to obtain the flowfield properties for the $\epsilon = 100$ nozzle for stagnation pressure $p_0 = 130$ psia and $\gamma = 1.4$. At this stagnation pressure, the thrust $F = 6.2$ lbf and $I_{sp} = 232$ lbf-s/lbm. A modified method-of-characteristics procedure[9] made use of a local Monte Carlo method to calculate viscous transonic expansion around the nozzle lip. In this calculation, $\gamma = 1.35$ was used. Far-field density ratios, ρ/ρ_a vs θ, for these method-of-characteristics solutions are compared in Fig. 5a with similar source-flow predictions for both $\gamma = 1.35$ and 1.4. The boundary-layer mass flow rate used in these source-flow predictions, $\dot{W}_b/\dot{W} = 0.07$, was computed from viscous nozzle flow analyses. The comparison of density along the axis is shown in Fig. 5b for $\gamma = 1.4$. As shown in the figures, agreement of results is reasonable among the various methods.

Similar calculations of far-field density ratios and axial density variations for the $\epsilon = 300$ nozzle at a stagnation pressure of 60 psia, for which $F = 2.8$ lbf and $I_{sp} = 225$ lbf-s/lbm, are shown in Fig. 6. In this case $\gamma = 1.36$, and in the source-flow calculation $\dot{W}_b/\dot{W} = 0.12$ was used. Again, the agreement between the method-of-characteristics and source-flow calculations is reasonable.

An example of the source-flow method is given in application to an electrothermal thruster, with supersonic flow in the divergent nozzle strongly influenced by viscous and heat-loss effects. The combustion products are assumed to be completely decomposed, resulting in molecular weight $\mathfrak{M} = 10.7$ lbm/mole. In this case, given nonuniform flow properties at the nozzle exit yield the starting values needed in the source-flow method: thrust $F = 0.0356$ lbf, $I_{sp} = 309.5$ lbf-s/lbm, average stagnation temperature $\bar{T} \simeq 3000°$R, and $\gamma = 1.31$. For the given γ, $\bar{T}$, and $\mathfrak{M}$, the ideal specific impulse is $I_{sp,i} = 340$ lbf-s/lbm. Using Eq. (5) to determine β from the estimated ratio $I_{sp}/I_{sp,i} = 0.91$ yields $\beta = 40.4$. With the mass flow

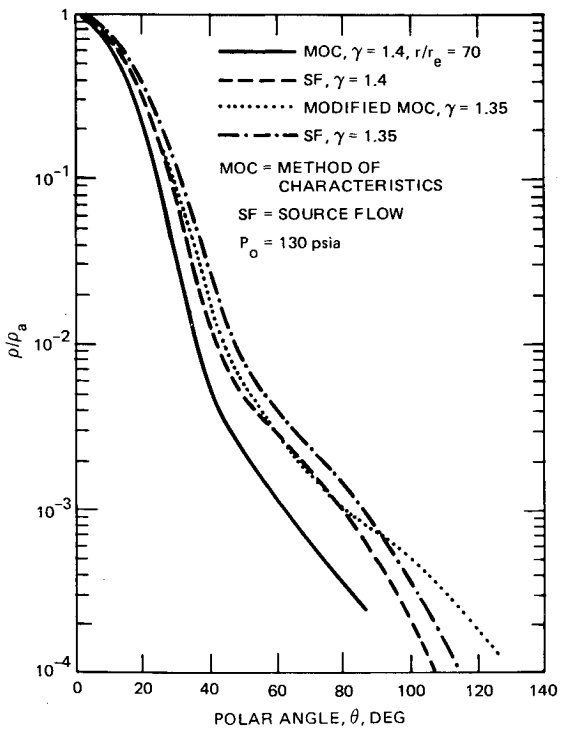

Fig. 5a Calculated far-field plume density ratio $\rho(r,\theta)/[\rho(r,0)] = \rho/\rho_a$ as a function of θ for nozzle area ratio $\epsilon = 100$.

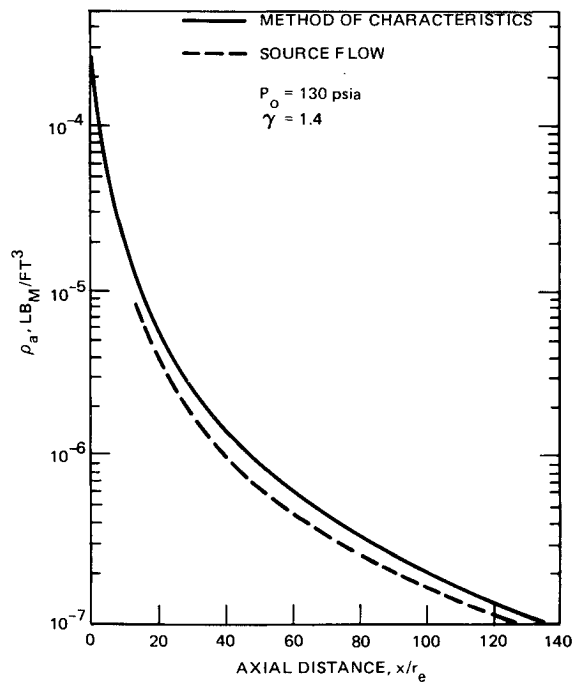

Fig. 5b Calculated density along plume axis for nozzle area ratio $\epsilon = 100$.

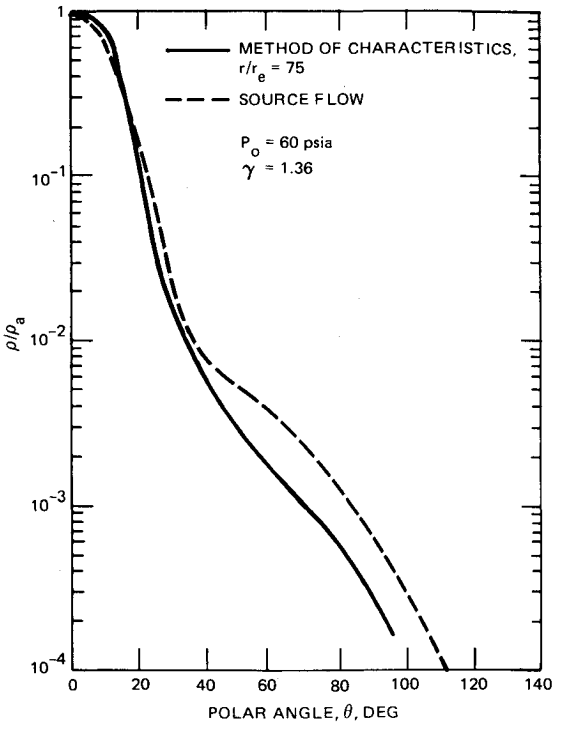

Fig. 6a Calculated far-field plume density ratio $\rho(r,\theta)/[\rho(r,0)] = \rho/\rho_a$ as a function of θ for nozzle area ratio $\epsilon = 300$.

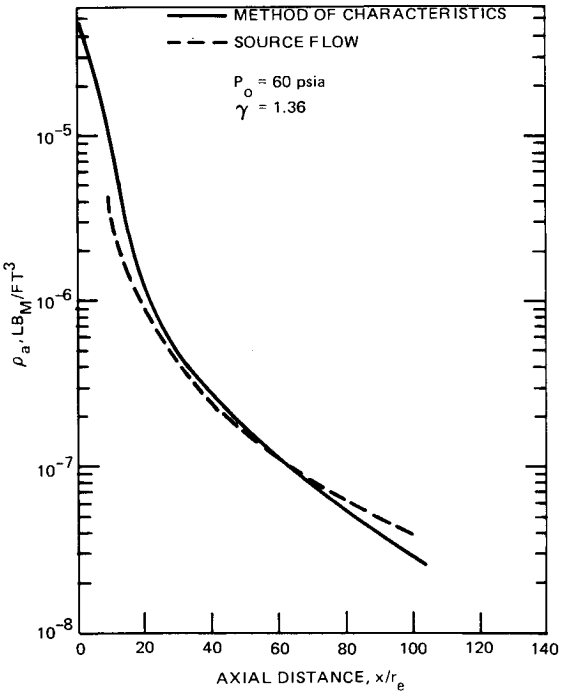

Fig. 6b Calculated density along plume axis for nozzle area ratio $\epsilon = 300$.

parameter $\alpha = 1.94 \times 10^{-4}$ lbm/s calculated from Eq. (2) and $V_m = gI_{sp,i} = 10{,}950$ ft/s, the far-field density for the electrothermal thruster based on Eq. (1) becomes

$$\rho(r,\theta) = \frac{1.77 \times 10^{-8}}{r^2}\left(\cos\frac{\theta}{2}\right)^{40.4} \text{lbm/ft}^3 \qquad (12)$$

where r is in feet.

Plume Shear Loss Calculations

For the 5-lbf thruster, the impingement areas on the HS 376 solar panel are generally in the transitional flow regime. Using the procedure for this regime as described in Sec. II, the bridging relation shown in Fig. 4 yields a significant reduction by a factor of about 4–5 in the flow shear when compared with free molecule shear employing Newtonian impact. Knudsen numbers, Kn, required in Fig. 4, are determined by use of kinetic theory formulas applicable to the hydrazine-decomposition products. The results for the percentage shear loss $\Delta F_\tau/F$ due to the previously presented plumes (see Figs. 5 and 6) are summarized in Table 2.

To obtain an assessment of transitional flow effects without using Fig. 4, a calculation was made for the $\epsilon = 300$ nozzle by applying the Monte Carlo GAPS code in an axisymmetric thruster/spacecraft configuration. This configuration is dic-

Table 2 Calculated plume shear loss $\Delta F_\tau/F$,%

MOC	4.05	3.66
SF	5.30	5.22
Inputs common to MOC and SF		
ϵ	100	300
p_0, psia	130	60
γ	1.4	1.36
$\mathfrak{M}$, lbm/mole	12.7	11.7
Inputs unique to SF		
β	75.2	115.8
β_b	8.8	8.3
V_m, ft/s	7851	7482
$\dot{W}_b/\dot{W}_b$	0.07	0.12

tated by the limitation of axial symmetry in the GAPS code. With a centered thruster in the solar panel, the Monte Carlo method yields a shear loss of 3.22%.[10] The corresponding method-of-characteristics (MOC) and source-flow (SF) percentages using Fig. 4 are 2.99 and 4.43%, respectively. Again, as in the operational thruster/spacecraft configuration, the reduction from free-molecule plume shear levels is about a factor of 4. Base pressure derived using the Monte Carlo method appears negligible, as found also by the other methods.

With respect to shear loss effects from the low mass flow electrothermal plume represented in Eq. (12), the lateral spreading of the plume results in a surface impingement within the solar panel equal to 38% of the total flow. The related free-molecule impact loss represents 35% of the thrust with only a minor influence of transitional effects, which reduces this loss to 28% of the thrust. However, because of the relatively large surface impingement in the nearly free-molecule flow regime, the backscatter of impinging molecules may contribute a significant base thrust in this case. Assuming diffuse internal reflection of molecules at the surface temperature of $T_s \simeq 600°$R, the base thrust recovery is estimated at 6% resulting in a calculated net loss of $\Delta F_\tau/F \simeq 22\%$. It is concluded that the high I_{sp} advantages of the low-pressure electrothermal thruster cannot be realized in the HS 376 solar panel configuration.

Comparisons with Flight Data

The shear loss predictions for the Hughes 5-lbf thruster with the $\epsilon = 100$ nozzle were compared with available flight data on axial thruster performance obtained from three operational HS 376 spacecraft.[11] The shear thrust loss component was deduced by comparing actual flight ΔV's following axial thruster firings (both pulsed and steady state) with the expected baseline ΔV's defined by the thruster acceptance test procedures. Based on these comparisons, the axial thruster mean thrust loss percentage was deduced as 6% with a standard deviation of $\pm 1\%$ for two of the spacecraft. The thrust loss, however, tended to decrease with increased mission lifetime, probably due to a systematic improvement in maneuver planning and data reduction techniques. Therefore, the final mean thrust loss percentage is believed to be 5%. The third spacecraft, on the other hand, showed a mean thrust loss percentage of 3% with a standard deviation of $\pm 0.6\%$. The initial interpretation of relatively meager data for this spacecraft leads to the conclusion that data that would be obtained over a longer mission lifetime would show a mean thrust loss percentage closer to 4%. Since the geometries of the three HS 376 spacecraft are identical, the current best evaluation of flight thrust loss yields values in the range of 4–5%. This estimate compares favorably with the $\epsilon = 100$ nozzle percentage shear loss predictions of 4.05% by the method of characteristics and 5.30% by the source-flow method. This comparison also tends to confirm the Monte Carlo prediction of negligible base pressure contribution to thrust loss. It should be recalled that the installed thrust loss is composed of plume shear loss (as modified by the base pressure contribution) ΔF_τ and the geometric thruster cant angle loss ΔF_δ, and that in the previous comparisons the geometric cant angle loss was consistently excluded.

IV. Concluding Remarks

The three analytical approaches used to describe the 5-lbf thruster hydrazine-decomposition plume yield relative differences which are typical of plume property predictions using state-of-the-art techniques. In deriving the integrated impingement effects on the extended surfaces of the HS 376 cylindrical solar panel, these relative differences in local density values become unimportant, and consistent shear loss predictions agree closely with spacecraft flight data. For the thruster spacecraft configuration considered, the impingement occurs predominantly in the transitional flow regime on the concave target surface. Use of the bridging relationship of Ref. 5, which leads to shear reducion by a factor of 4–5 from free-molecule Newtonian shear appears to be corroborated by a Monte Carlo calculation independent of the bridging relation.

A novel feature of the source-flow method used in the analyses is worth noting. The present source-flow formulation allows for the possibility of realistic far-field predictions by explicit use of two basic propulsion test data, when available (e.g., see Ref. 12 for C_F correlations): 1) c^* efficiency, which accounts for combustion chamber losses and is the principal factor in determining the far-field flow velocity V_m, and 2) C_F, which contains the effects of nozzle design, and boundary-layer momentum and heat-transfer losses implied by finite β.

Appendix

From the source-flow description of the far-field density, $\rho(r,\theta)$, in Eq. (1) the total mass flow rate $\dot{W}$ and thrust F can be expressed by using conservation laws as

$$\dot{W} = 2\pi V_m \int_0^\pi \rho r^2 \sin\theta \mathrm{d}\theta$$

$$= 2\pi\alpha \int_0^\pi \left(\cos\frac{\theta}{2}\right)^\beta \sin\theta \mathrm{d}\theta$$

$$F = 2\pi \frac{V_m^2}{g} \int_0^\pi \rho r^2 \sin\theta \cos\theta \mathrm{d}\theta$$

$$= 2\pi \frac{V_m}{g} \alpha \int_0^\pi \left(\cos\frac{\theta}{2}\right)^\beta \sin\theta \cos\theta \mathrm{d}\theta \qquad \text{(A1)}$$

In Eq. (A1) the thrust has been expressed as the reaction of the momentum flow in the axisymmetric far field. Evaluation of the integrals yields

$$\dot{W} = \frac{8\pi\alpha}{\beta+2}$$

$$F = \frac{8\pi\alpha\beta V_m/g}{(\beta+2)(\beta+4)}$$

$$I_{sp} = \frac{F}{\dot{W}} = \frac{\beta V_m/g}{\beta+4}$$

and additional results quoted in Sec. II. In particular, the reduced density distribution, Eq. (6), depends only on β, for which numerical values have been calculated using Eqs. (5), (7), and (8), as plotted in Fig. 3.

Combination of the boundary-layer flow and the inviscid flow in the far field involves two sets of α,β parameters, which

upon elimination can be reduced to the form

$$\rho(r,\theta)=\frac{\beta+2}{8\pi}\frac{(\dot{W}-\dot{W}_b)}{V_m r^2}\Big/\left(\cos\frac{\theta}{2}\right)^{\beta}$$

$$+\frac{\beta_b+2}{8\pi}\frac{\dot{W}_b}{V_m r^2}\left(\cos\frac{\theta}{2}\right)^{\beta_b}$$

where the β_b of the boundary-layer flow component has been calculated for sonic flow, i.e., $\epsilon=1$. The preceding density is used in Eq. (9) for calculating the shear loss ΔF_τ in the source-flow description of the combined flows.

Acknowledgment

The authors are grateful to Dr. J.E. Chirivella of Ergo-Tech Systems Inc., Tujunga, California, for his many valuable contributions to this effort.

References

[1]Deissler, R.G. and Loeffler Jr., A.L., "Analysis of Turbulent Flow and Heat Transfer on a Flat Plate at High Mach Numbers with Variable Fluid Properties," NASA TR R-17, 1959.

[2]Whitfield, D.L., "Viscous Effects in Low Density Nozzle Flows," AEDC TR-73-52, June 1973.

[3]Sutton, G.P. and Ross, D.M., *Rocket Propulsion Elements*, John Wiley & Sons, New York, 1976, p. 66.

[4]Sibulkin, M. and Gallaher, W.H., "Far-Field Approximation for a Nozzle Exhausting into a Vacuum," *AIAA Journal*, Vol. 1, June 1963, pp. 1452–1453.

[5]Matting, F.W., "Approximate Bridging Relation in the Transitional Regime Between Continuum and Free-Molecule Flows," *Journal of Spacecraft and Rockets*, Vol. 8, Jan. 1971, pp. 35–40.

[6]McGregor, R.D., "Users Manual for the TRW 'GAPS' Computer Program for the Analysis of Gas Exhaust-Plume Flowfields Using the Direct Simulation Monte Carlo Method," TRW, Redondo Beach, CA, Contract No. 955487, May 1980.

[7]Bird, G.A., *Molecular Gas Dynamics*, Clarendon Press, Oxford, 1976.

[8]Mirels, H. and Mullen, J.F., "Expansion of Gas Clouds and Hypersonic Jets Bounded by a Vacuum," *AIAA Journal*, Vol. 1, March 1963, pp. 596–602.

[9]Chirivella, J.E., "Maximum Thrust Nozzle Contour Analysis," Ergo-Tech Systems, Tujunga, CA, Rept. ER-SP-1001, Aug. 1983.

[10]Chirivella, J.E., "Monte Carlo Estimate of the HS 376 Plume Impingement Losses," Ergo-Tech Systems, Tujunga, CA, Rept. ER-SP-1004, Oct. 1984.

[11]Chirivella, J.E., "SBS-1, -2, -3 Thruster Performance-Flight Data Analysis," Ergo-Tech Systems, Tujunga, CA, Rept. ER-SP-1003, June 1984.

[12]"Liquid Rocket Engine Nozzles," *NASA Space Vehicle Design Criteria Monograph*, NASA SP-8120, July 1976, p. 14.